

Comparison of interfacial and critical current behaviour of Al+Al₂O₃ sheathed MgB₂ wires with Ta and Ti diffusion barriers

S. Santra^{a,*}
sangeeta.santra@gmail.com

C.R.M. Grovenor^a

S.C. Speller^a

P. Kováč^b
pavol.kovac@savba.sk

L. Kopera^b

I. Hušek^b

^aDepartment of Materials, University of Oxford, Oxford, OX1 3PH, United Kingdom

^bDepartment of Superconductors, Institute of Electrical Engineering of SAS, Bratislava, Slovakia

*Corresponding author.

Abstract

We present a comparative study of the interfacial reactions for the MgB₂ wires with different diffusion barriers (Ta or Ti) and the outer (Al + Al₂O₃) sheath with variable Al purity and Al₂O₃ content. The reaction of (Al + Al₂O₃) with Ta produces non-uniform but considerably thinner interfacial layer than with Ti. The critical currents (I_c) of the MgB₂ wires with Ta barrier do not vary any significantly for different heat treatment conditions, and in contrast, those with Ti barrier show a strong variation with Al purity and volume % of Al₂O₃ particles in the (Al + Al₂O₃) sheath. For the (Al + Al₂O₃) sheathed wire with Ti barrier, the maximum I_c is attained when the highest purity of 99.995% Al is used although the thickest reaction zone has developed at the Ti-(Al + Al₂O₃) interface. The critical current values suggest that not the interfacial reaction kinetics of barrier-sheath rather the purity of the Al powder and the volume % of Al₂O₃ particles in sheath determine the current carrying ability of the MgB₂ composite wires. The current-voltage characteristics of wires when combined with the reaction behaviour at barrier-sheath interfaces, the (Al + Al₂O₃) sheathed MgB₂ wires with Ti diffusion barrier looks more promising than Ta for engineering applications.

Keywords: Composite MgB₂ superconductors; Solid state interfacial reactions; Thermal stability; Critical current

1 Introduction

The intermetallic magnesium diboride (MgB₂) superconductor compound has higher critical temperature (T_c) of 39 K than the conventional low temperature superconductors [1]. It also offers advantages of larger coherence length (~5 nm), absence of weak-link at the grain boundaries [2], cost-effectiveness [1] and almost an isotropic behaviour [3]. As a result, manufacturing MgB₂ wires with high critical current is of scientific interest for various engineering applications [4,5]. The effective process for producing nearly stoichiometric and dense MgB₂ wires is the internal magnesium diffusion (IMD) technique [6]. In the IMD technique, a solid magnesium (Mg) rod is surrounded by the boron powder, and the MgB₂ compound forms when Mg infiltrates into the boron (B) compacted powder [6].

The MgB₂ wires should be stabilized thermally by a highly conductive metal, and be able to provide the mechanical strength [7]. Cu is used as the outer stabilizing sheath for the commercially produced NbTi and Nb₃Sn superconducting wires [8]. However, the Cu-sheathed MgB₂ composite wire produces a deleterious Cu₂Mg layer at the MgB₂-Cu interface [9], and therefore the transport current density decreases [10]. Research demonstrates that the high thermal and electrical conductivity of Al can be put to use for an outer stabilizer sheath, and is mechanically reinforced too, when alloyed with ultrafine grained Al₂O₃ [11].

It is important that the stabilizer sheath material does not react with the formed MgB₂ and produce any reaction layer which often can be non-superconductive, and as a result, the current carrying properties of the MgB₂

composite wire may deteriorate [3,12]. Therefore, an intermediate diffusion barrier is used to avoid, or minimize reaction between MgB_2 filaments and the outer ($\text{Al} + \text{Al}_2\text{O}_3$) stabilizer sheath. Additionally, the diffusion barrier material should itself be chemically unreactive with either Mg or B, which otherwise may decrease the fraction of the superconducting compound, MgB_2 [3]. Few metallic elements have been explored for the role of an intermediate diffusion barrier such as Fe [13], Nb, Ta, Ti [7,14]. Fe and Nb react with MgB_2 , and form Fe_2B and Nb(B) solid solution respectively which consumes some portion of the B at the initial stage of heat treatment, and consequently results in a reduced cross-sectional area of MgB_2 [13]. Although both the commercial powder-in-tube (PIT) MgB_2 wires [15,16] and high J_c IMD MgB_2 wires [17,18] are using thin Nb barrier to decrease its reaction with B to achieve reasonable critical current values [13], MgB_2 wire with Ti barrier provides higher critical current density than with Nb by a factor of two. Additionally, Nb may not be a good option to be used as a barrier with $\text{Al} + \text{Al}_2\text{O}_3$ sheath because of higher reaction kinetics between Nb and Al [7]. On the other hand, the sufficiently ductile Ta is reported to show a minimal reactivity with Mg [10]. Few authors of this article have found that Ti offers the best core uniformity and the highest powder density prior to the heat treatment among the others [19], and produces a superconducting wire which is considerably lighter when combined with the ($\text{Al} + \text{Al}_2\text{O}_3$) stabilizer sheath [10]. However, a detailed analyses on the reactions between MgB_2 -barrier (Ta or Ti) and barrier-($\text{Al} + \text{Al}_2\text{O}_3$) stabilizer sheath are yet to be addressed.

This paper aims to study the effect of elemental diffusion barriers Ta and Ti on the interfacial reactions with the outer ($\text{Al} + \text{Al}_2\text{O}_3$) stabilizer sheath of variable Al purity and particle size of Al_2O_3 . The critical temperature of MgB_2 and transport properties of the MgB_2 composite wires are determined and discussed in view of the MgB_2 formation and the reactions at the diffusion barrier-stabilizer sheath interfaces which depends on the processing variables. The current-voltage, I - V , characteristics of the MgB_2 composite wires are also studied, and the thermal stabilities of the wires with Ta and Ti barriers are compared.

2 Experimental procedure

Single-core MgB_2 wire was composed of pure Mg wire of 2.94 mm in diameter surrounded by amorphous boron powder (99.8 wt% pure, 50–450 nm, filled in glove-box) inside the Ta (or Ti) tube of 5.55 mm (or 7.11 mm). The packing density of the boron powder was below 50% because of hand densification by a metallic tube around the Mg central wire in a glove box with Ar atmosphere. Mg/B/Ta and Mg/B/Ti composites were swaged to 5.99 mm, and inserted into the $\text{Al} + \text{Al}_2\text{O}_3$ tubes of 6.29 mm and 9.1 mm respectively, and groove rolled up to a rectangular wire of $\sim 1.1 \times 1.1 \text{ mm}^2$. Internal Mg diffusion into B was done during the final heat treatment under argon atmosphere at 635 °C for 8 min (HT1) by ramping at a higher rate and at 645 °C for 20–60 min (HT2), see Fig. 1. As one can see, the maximum temperatures of HT1 and HT2 are different and close to the melting point of Mg core (650 °C), and also closer to the melting point of ($\text{Al} + \text{Al}_2\text{O}_3$) sheath (~ 652 °C), and the heat treatment conditions for three wires with Ta barrier (W_{Ta}) are listed in Table 1a. Three different ($\text{Al} + \text{Al}_2\text{O}_3$) sheaths are used for wires with Ti barrier (W_{Ti}) fabricated by the same process. The ($\text{Al} + \text{Al}_2\text{O}_3$) sheaths were made by powder metallurgy from aluminium powders of different purity 99.9–99.995% and particle size between 0.8 μm and 3.0 μm , for the details of the corresponding wires please refer Table 1b. Very small amount of metallic impurities (e.g. Ni) in Al powder of purity 99.9% was present, which was not quantified. The final heat treatment was done under argon atmosphere for the wires with Ti barrier at 640 °C for 60 min (with short overheating to $T_{\text{max}} = 647$ °C/5min).

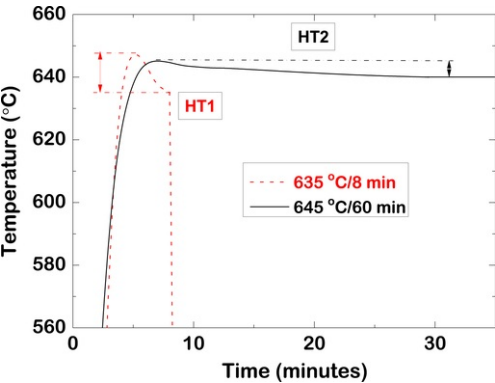


Fig. 1 Typical heat treatment profiles HT1 and HT2 applied for the ($\text{Al} + \text{Al}_2\text{O}_3$) sheathed composite MgB_2 wires.

alt-text: Fig. 1

Table 1 Description of (a) $\text{MgB}_2/\text{Ta}/\text{Al}+1.5 \text{ vol}\% \text{ Al}_2\text{O}_3$ samples annealed at different conditions, and (b) $\text{MgB}_2/\text{Ti}/\text{Al} + \text{Al}_2\text{O}_3$ samples annealed at 640 °C for 60 min (HT2) and differing by the outer sheath.

alt-text: Table 1

Sample	W_{Ta}^1	W_{Ta}^2	W_{Ta}^3

Temperature (°C)	635	645	645
time (minutes)	8 (HT1)	20 (HT2)	60 (HT2)
Sample	W_{Ti}^1	W_{Ti}^2	W_{Ti}^3
Al purity (%)	99.995	99.9	99.9
Al ₂ O ₃ (vol %)	1.6	1.5	3.1
d ₅₀ of Al ₂ O ₃ (µm)	1.9	3.0	0.8

The wired samples were cross-sectioned transversely, mounted on a steel clip and embedded in conductive powder. The mounted samples were first dry grinded on silica polishing sheets of different grades, and fine polished using diamond paste of 1 µm particle suspension. The composition analyses of the samples were conducted in a field-emission gun based scanning electron microscope (SEM) equipped with an energy dispersive X-ray spectrometer (EDXS). The average compositions of the phases were determined by analysing ten different locations of the interfacial regions, and the reaction zones were mapped to probe the elemental distribution in the respective phases. The entire annular barrier-(Al + Al₂O₃) interface was checked to estimate an average thickness of the reaction zone using the Image J software.

The resistive transitions were measured by a standard four-probe method with DC current magnitude of 100 mA to determine the critical transition temperature (T_c) of MgB₂ and compare the resistance behaviour of different composite wires. To quantify the thermal stability of presented wires, *I*-*V* characteristics with the constant current ramping (up and down) at 0.43 As⁻¹ above the *I*_c criterion were measured and compared. Transport critical currents were measured at the liquid helium temperature and in an external magnetic field from 4 T up to 8 T using standard DC measurement with 1 µVcm⁻¹ criterion.

3 Results and discussion

We have first discussed the reaction zones developed at the Ta-(Al + Al₂O₃) interfaces of different wires, and compared their kinetics with the heat treatments followed in our study. Following, we have compared the characteristics of the reaction layers at the Ti-(Al + Al₂O₃) interfaces in view of different purity of Al and particle size of Al₂O₃. We have also discussed about the formation of the reaction zones at the Mg-MgB₂-barrier interfaces with a focus on the superconducting phase layer, and correlated with the critical transition temperatures of MgB₂ for selected wires. The measured critical current (*I*_c) values and current-voltage (*I*-*V*) characteristics of all the MgB₂ wires have been compared, and correlated with the interfacial behaviour of the diffusion barrier-(Al + A₂O₃). To have an idea about the design of the composite wire, we have presented a transverse cross-section of a heat treated wire in the *graphical abstract*.

3.1 Interfacial reactions

3.1.1 Ta - (Al + Al₂O₃) interfaces

The reaction between Ta and (Al + Al₂O₃) for all the wires results in the most Al-rich intermetallic phase [20], TaAl₃, and have irregular phase boundaries at either of the sides. Fig. 2 shows the back-scattered electron (BSE) micrographs for the W_{Ta}^1 , W_{Ta}^2 and W_{Ta}^3 wires illustrating the reaction zones at the Ta-(Al + Al₂O₃) interfaces. The TaAl₃ phase has the least thickness of ~1 µm in W_{Ta}^1 , and has formed in dispersed manner towards Ta-rich sheath, as highlighted by ‘1’ in Fig. 2a. The layer thickness of TaAl₃ has increased to ~3 µm for the wires W_{Ta}^2 and W_{Ta}^3 , which have been heat treated at higher temperatures, however, the irregularities in the phase boundaries persist in these wires. One can notice in Fig. 2b that the TaAl₃ phase exhibits finger-like feature protruding towards the Ta-rich side for W_{Ta}^2 .

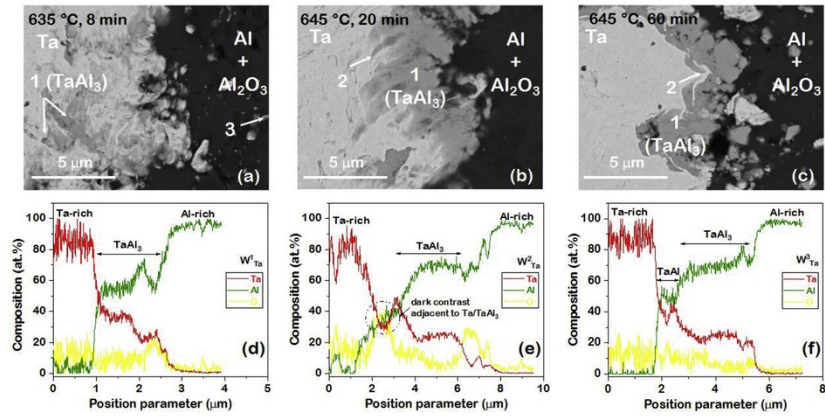


Fig. 2 (a-c) Back-scattered electron (BSE) micrographs showing the reaction zones at the Ta-(Al + Al₂O₃) interfaces for the W_{Ta}^1 , W_{Ta}^2 and W_{Ta}^3 wires respectively, (d-f) along with the corresponding composition profiles.

alt-text: Fig. 2

Combining the results of the composition profiles and elemental maps displayed in Fig. 2d-f and 3a-b respectively, we find the TaAl phase to form only at intermittent regions of the Ta/TaAl₃ interface for the wires, W_{Ta}^2 and W_{Ta}^3 , which were heat treated at higher temperature. It is possible that the TaAl phase in W_{Ta}^1 either has not formed, or if present, must be too small to detect in view of lower temperature and shorter time. The presence of TaAl, denoted by '2', is featured in Figs. 2 and 3, and is demarcated on the composition profiles, Fig. 2e and f. The Ta-TaAl₃ interface, highlighted by a dotted white box in Fig. 3a, indicates that some amount of oxygen is soluble in the TaAl phase than in TaAl₃. The solubility of oxygen in TaAl is also corroborated by the darker contrast of the TaAl phase than TaAl₃, see Fig. 2b. However, the thickness is too small to quantify the O-solubility in the TaAl phase. The elemental map of Ta (Fig. 3b) indicates that few Ta-rich oxide particles denoted by '3' are present in the (Al + Al₂O₃) sheath for all the samples.

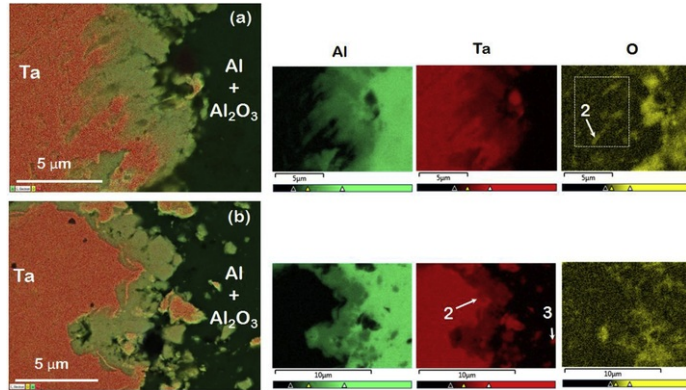


Fig. 3 Elemental composition maps showing the distribution of Al, Ta and O in the reaction phase layers developed at the Ta-(Al + Al₂O₃) interfaces for the (a) W_{Ta}^2 and (b) W_{Ta}^3 wires.

alt-text: Fig. 3

3.1.2 Ti - (Al + Al₂O₃) interfaces

In contrast to the Ta barrier, considerably thicker interfacial phase layers have developed on reaction between Ti and (Al + Al₂O₃) sheath, and are present continuously throughout the annular Ti-(Al + Al₂O₃) regions for the wires W_{Ti}^1 , W_{Ti}^2 and W_{Ti}^3 . Fig. 4a-c shows the reaction zones developed at the Ti-(Al + Al₂O₃) interfaces in a series of BSE micrographs. Similar to the wires with Ta barriers, those with Ti barrier, too, produces the most Al-rich intermetallic phase [20], TiAl₃, as the major phase and is denoted by '1' in Fig. 4. The TiAl₃ phase grows with a small homogeneity range with a fixed Ti content of ~25 at.% in accord to the binary Ti-Al phase diagram [20]. The Al + Al₂O₃ sheath with the highest purity of 99.995% Al produces the thickest TiAl₃ phase layer of $38 \pm 0.5 \mu\text{m}$. Those with lesser purity of 99.9% Al results in a decrease in the layer thickness of TiAl₃ with $14 \pm 1.6 \mu\text{m}$ and $13 \pm 0.8 \mu\text{m}$ in W_{Ti}^2 and W_{Ti}^3 respectively, and the interface appears serrated too. The cracks in the TiAl₃ phase for the W_{Ti}^1 may have generated because of the stress accumulated owing to the volume mismatch on phase growth, or possibly due to the coalescence of the Kirkendall pores near the Al-rich side since Al is reported to be the faster diffusing species

through the growing TiAl_3 phase [21]. The critical thickness of the TiAl_3 phase has possibly not been attained for the crack to initiate in W_{Ti}^2 and W_{Ti}^3 .

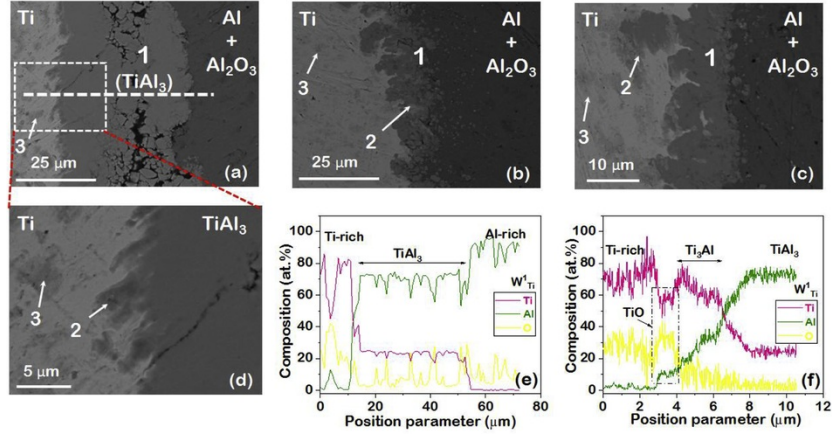


Fig. 4 Back-scattered electron (BSE) micrographs showing the interfacial reaction zones at the (a-c) Ti-(Al + Al_2O_3) for the W_{Ti}^1 , W_{Ti}^2 and W_{Ti}^3 wires respectively, and (d) Ti- TiAl_3 for W_{Ti}^1 . Composition profiles across the developed reaction zones at the (e) Ti-(Al + Al_2O_3) and (f) Ti- TiAl_3 interfaces for W_{Ti}^1 .

alt-text: Fig. 4

A close inspection of the Ti- TiAl_3 interface in W_{Ti}^1 reveals that a very thin phase layer has also formed which is denoted by '2' in Fig. 4d. The composition of the phase '2' corresponds to the Ti-rich $(\text{Ti},\text{O})_3\text{Al}$ phase. The composition profile in Fig. 4f indicates Ti_3Al to have a homogeneity range in accord to the Ti-Al phase diagram [20]. The Ti_3Al phase has a solubility of ~ 10 at.% O in contrast to oxygen free TiAl_3 , which is clearly deduced from the elemental map of oxygen in Fig. 5b. Referring to the Al-Ti-O isothermal section at 945°C [22], the solubility limit of O in the Ti_3Al phase is considerably higher than that in TiAl_3 . Although the isothermal section is at a temperature higher than the one used in our study, we can say that the trend in the solubility limit of oxygen in the Ti-Al based phases will be maintained at the lower temperature as well. Furthermore, the solubility lobe of $(\text{Ti},\text{O})_3\text{Al}$ phase is inclined towards the Al-rich side, thereby indicating that O prefers to occupy the Ti-sublattice in Ti_3Al . Preference of O to Ti can be deduced from the spot analysis, where the total (Ti + O) amounts to ~ 75 at.% (please refer Fig. 4f). Spot '3' corresponds to the TiO phase with little solubility of ~ 2 at.% Al which is dispersed randomly within the Ti barrier, as marked in Fig. 4a-d. Such an oxide phase is, however, not observed in the wires with Ta barrier.

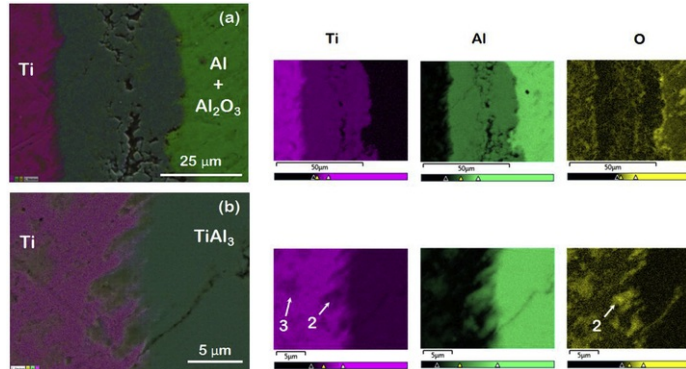


Fig. 5 Elemental composition maps showing the distribution of Al, Ti and O in the reaction phase layers developed at the (a) Ti-(Al + Al_2O_3) and (b) Ti- TiAl_3 interfaces for W_{Ti}^1 .

alt-text: Fig. 5

By comparison, we confirm that the interfacial reaction zones formed at the barrier-(Al + Al_2O_3) interfaces are considerably thinner and non-uniform when Ta diffusion barriers are used than for those with Ti barriers.

3.1.3 Mg - (diffusion barrier Ta or Ti) interfaces

The Mg wire, surrounded by the compacted B powder, reacts with B to form an annular region of MgB_2 along the inner surface of the barrier during the heat-treatment of the as-drawn wires. Fig. 6 shows the BSE micrographs focussing the interfacial regions of Mg-MgB₂-Ti. It is the MgB_2 phase highlighted by spot '1' in Fig. 6a-c that offers superconductivity at the temperatures below its T_c of 39 K [1]. The dense MgB_2 layers formed in all these samples contain almost no porosity. This is an added advantage of employing IMD technique for producing MgB_2 than the commonly practiced powder-in-tube (PIT) method where the formed MgB_2 has relatively higher fraction of pores [6]. The MgB_2 phase is $\sim 100\ \mu\text{m}$ thick, and has nearly a homogeneous composition of 34 at.% Mg and 66 at.% B in all the wires as determined from the average composition of spot analysis at ten different random locations inside the MgB_2 phase layer, and depicted in the composition profiles shown in Fig. 6d-f.

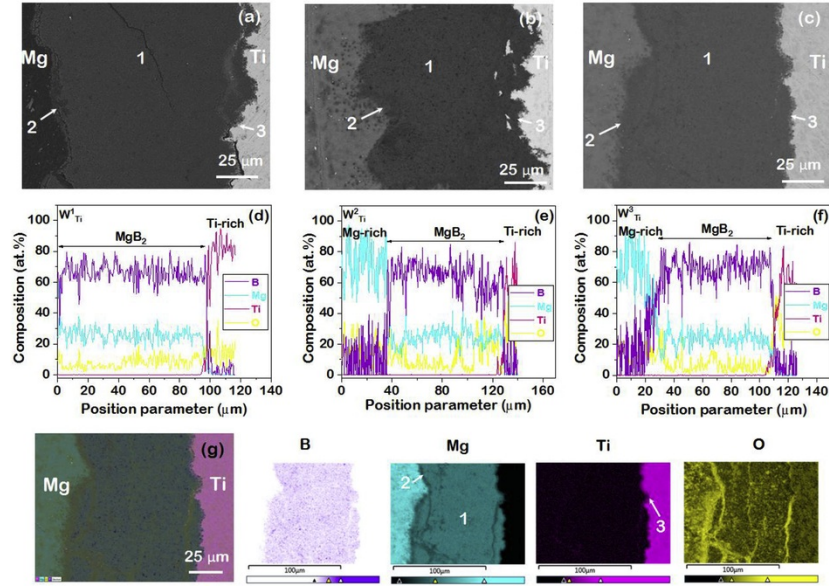


Fig. 6 (a-c) Back-scattered electron micrographs showing the Mg-MgB₂-Ti interfaces in the wires, W_{Ti}^1 , W_{Ti}^2 and W_{Ti}^3 , (d-f) and the corresponding composition profiles. (g) Composition EDXS map showing the distribution of different elements across the formed MgB_2 phase layer

alt-text: Fig. 6

Two very thin phase layers have developed on either side of the MgB_2 phase, and are present as continuous layers at the Mg-MgB₂ and MgB₂-Ti interfaces. The elemental composition maps focussing the Mg-MgB₂-Ti interfaces is shown in Fig. 6g to have a clear view of the thin phase layers. The phase denoted by '2' is MgO, and one can observe a higher amount of oxygen in '2' than in MgB_2 in the composition map of oxygen. Certain regions appear to have picked up strong oxygen peaks which correspond to the cracked portions. The elemental composition map of Ti (Fig. 6g) shows that the phase denoted by '3' is 3 μm thick what we presume is a ternary B-Mg-Ti compound with ~ 50 at.% B and ~ 12 at.% Ti. It is worthy to mention that the MgB_2 phase shows no solubility of Ti. These three phases at the Mg-barrier interface is very characteristics of all the wires with Ti barrier.

In contrast to the Ti-containing phase at the MgB₂-Ti interface, neither of the wires with Ta diffusion barrier shows any sort of interaction at the MgB₂-Ta interface. The phase, MgB_2 , can be observed in Fig. 7a-c with nearly no oxygen dissolution, see the elemental map in Fig. 7g. The developed MgB_2 phase in all the wires with Ta barrier show good homogeneity with ~ 66 at.% B and 34 at.% Mg. The MgO phase denoted by '2' in Fig. 7a-c has formed in the wires with Ta diffusion barrier too, similar to those with Ti as the barrier. As one can notice, the MgB_2 phase layer formed in W_{Ta}^3 is not as compact as those of W_{Ta}^1 and W_{Ta}^2 , and the non-uniformity might have been caused as a result of metallographic preparation, or strain accumulation due to the heat treatment for longer annealing times.

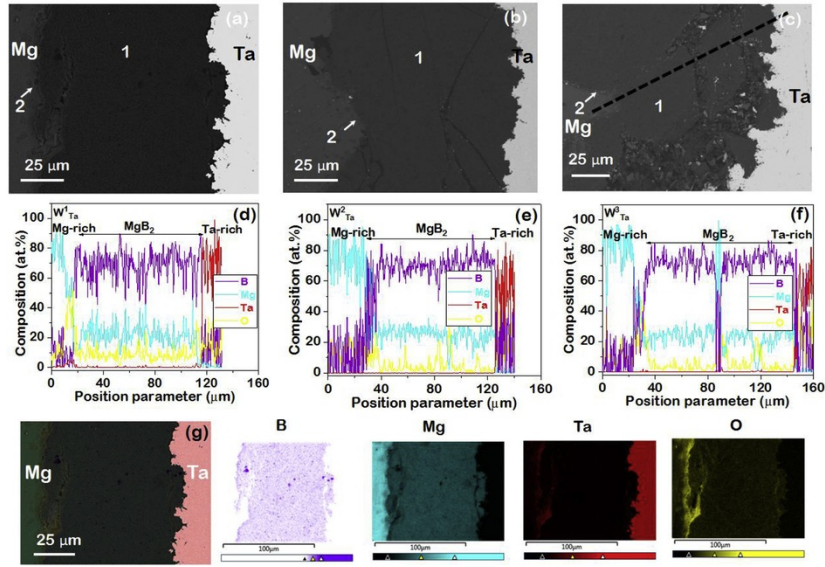


Fig. 7 (a-c) Back-scattered electron micrographs showing the Mg-MgB₂-Ta interfaces in the wires, W_{Ta}^1 , W_{Ta}^2 and W_{Ta}^3 , (d-f) and the corresponding composition profiles. (g) Composition EDXS map showing the distribution of different elements across the formed MgB₂ phase layer in W_{Ta}^1 .

alt-text: Fig. 7

To examine if there is any effect of the heat treatment conditions or variables of (Al + Al₂O₃) sheath on the compositional homogeneity of the MgB₂ phase, we have determined the critical transition temperatures for few selected wires. The current carrying properties and thermal stabilities of the composite MgB₂ wires with Ta or Ti diffusion barrier were evaluated and correlated with the interfacial reaction kinetics of barrier-(Al + Al₂O₃) sheath.

3.2 Superconducting properties

3.2.1 Critical temperatures and $R(T)$

Fig. 8a compares the resistive critical temperature measurements for the W_{Ta}^1 , W_{Ta}^3 and W_{Ti}^2 wires. W_{Ti}^2 has the same volume % of Al₂O₃ (1.5) as those of with Ta barriers. The transition width ($\Delta T_c \sim 2$ K) is nearly the same for W_{Ta}^1 , W_{Ta}^3 and W_{Ti}^2 , because of similar superconducting phase purity for the formed MgB₂ phase. W_{Ta}^3 which was heat treated at the highest temperature (645 °C) for longer time (60 min) has the highest T_c of ~ 38.5 K. The T_c of 38.5 K is pretty closer to the T_c of the stoichiometric MgB₂ compound [1]. Heat treated for a longer time may have helped to reach the composition of MgB₂ closer to its stoichiometry for W_{Ta}^3 . On the other hand, W_{Ti}^2 which was heat treated at 640 °C for 60 min has a lower T_c of 38 K than W_{Ta}^3 but higher than W_{Ta}^1 which was heat treated at 635 °C for 8 min. The trend in T_c of IMD processed MgB₂ reflects the influence of heat treatment on T_c .

The substantial microstructural changes that (Al + Al₂O₃) sheath material undergoes gradually from as-deformed (AD) through heat treated (HT) affects the electrical resistance of the MgB₂ composite wire. **Fig. 8b** compares the temperature dependent resistance, $R(T)$, from room temperature to 25 K for AD and HT wires with Ta and Ti barriers. One can observe that the resistance of the as-deformed wires increases after heat treatment. It is bit unusual because annealing encourages grain coarsening and reduction of defect density, and as a result, one would expect exactly the opposite. Therefore, an increase in resistance of the heat treated wires can be attributed to the interfacial reaction zones developed at the barrier-(Al + Al₂O₃) sheath. The reaction between the barrier material and stabilizer sheath is also reflected on the reduced residual resistivity ratio $RRR_{40} = RRR_{300\text{ K}}/R_{40\text{ K}}$ to 13.5 (W_{Ta}^1) and 10.7 (W_{Ta}^2), and 16.7 (W_{Ti}^2) from 17.4 of AD wire. In addition, different $R(T)$ characteristics are measured for the wires with Ta- and Ti-barrier in the range of 40–300 K. The W_{Ti}^2 wire shows the highest resistance at the room temperature, however, it decreases with temperature more radically compared to W_{Ta}^1 and W_{Ta}^2 , and reaches a minimum resistance at 40 K. One of the possible reasons could be purification of outer sheath by Ti barrier gathering impurities from (Al + Al₂O₃). One can also observe in **Fig. 4** that the oxide TiO phase is present in the Ti barrier but not in Ta. A detailed microscopy analysis is underway to understand the reason for relatively a steep decrease in the resistance with lowering of the temperature in the case of Ti barrier.

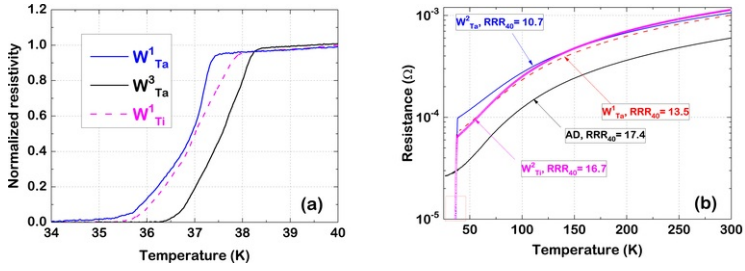


Fig. 8 (a) Resistive transitions of MgB₂-Ta-Al + Al₂O₃ and MgB₂-Ti-Al + Al₂O₃ wires heat treated at different conditions and (b) $R(T)$ dependences of annealed wires compared to as-deformed one.

alt-text: Fig. 8

3.2.2 Critical current and I-V characteristics of MgB₂ wires

To evaluate the current carrying ability of the (Al + Al₂O₃) sheathed MgB₂ wires, the critical current (I_c) values were determined as a function of magnetic fields from 4 T to 8 T at 4.2 K. Fig. 9a and b show the trend of I_c for the MgB₂ wires with the Ta and Ti barriers respectively, and with different processing variables. The I_c values of the wires with Ta or Ti barrier decrease (linearly-for semi-log plot or exponentially-for linear plot) with the magnetic field up to 8 T, and approach low current values of approximately 20 A at 8 T. For the wires with Ta barrier, the maximum I_c is attained for W_{Ta}^1 (~215 A at 5 T), and the minimum for W_{Ta}^3 showing a reduction by 13%. Therefore, we can say that the I_c values for W_{Ta}^1 , W_{Ta}^2 and W_{Ta}^3 lie within the error limits, and current carrying ability of the MgB₂ wires with Ta barrier is not so sensitive to the heat treatment conditions. Therefore, not a significant variation in the critical currents among the wires with Ta barrier can be attributed to the minute difference in the interfacial kinetics at the barrier-sheath interfaces (see Fig. 2) considering the fact that the thickness of MgB₂ is nearly the same irrespective of the heat treatment conditions and same processing variables for the stabilizer (Al + Al₂O₃) sheath. Furthermore, we have noted in the previous section that a maximum critical transition temperature of ~38.5 K for MgB₂ is achieved when heat treated at 645 °C for 60 min. Therefore, a balance of I_c and T_c can be obtained by changing the heat treatment conditions which can be decided depending on the applications.

In contrast to the wires with Ta barrier, we notice the critical current values to differ with different purity of Al in the (Al + Al₂O₃) sheathed wires with Ti barrier, see Fig. 9b. A maximum I_c of 202 A at 5 T is exhibited by W_{Ti}^1 , the one with highest purity of Al, though it shows the highest growth for the interfacial layer (Fig. 4a). The W_{Ti}^3 wire which has the highest volume fraction of the Al₂O₃ particles in the (Al + Al₂O₃) sheath shows the minimum I_c , and has reduced by 54% at 5 T although it produces the interfacial reaction zone of least thickness (Fig. 4c). In view of the similar MgB₂ layer thickness, therefore, we suggest that it is not the interfacial reaction kinetics between Ti and (Al + Al₂O₃) that governs the I_c rather the purity of Al in the stabilizer sheath. In addition, the I_c values converge to nearly the same I_c of ~17 A on approaching higher magnetic fields for W_{Ti}^2 and W_{Ti}^3 , which differ only by the volume fraction and particle size of Al₂O₃ in the outer stabilizer sheath. However, different volume fractions of Al₂O₃ influences the hardness of the (Al + Al₂O₃) sheaths in as-deformed and in annealed states too [23]. The micro-hardness, HV0.05, of (Al + Al₂O₃) sheaths measured in as-deformed condition and after heat treatment (AD/HT) were: 56/51 MPa for W_{Ti}^1 , 63/56 MPa for W_{Ti}^2 and 83/78 MPa for the W_{Ti}^3 wire. An increased volume fraction of Al₂O₃ leads to a mechanically stronger Al + Al₂O₃ sheath [23] and consequently, the densification of boron powder during the deformation step and the pressure stress induced in the MgB₂ phase after annealing is not the same for the wires, W_{Ti}^1 - W_{Ti}^3 , with Ti barrier and (Al + Al₂O₃) sheaths with different volume and particle size of Al₂O₃. Therefore, the volume % of Al₂O₃ particles in the (Al + Al₂O₃) sheath also plays a role in determining the critical currents of the composite MgB₂ wire, however not as significant as that of the purity of Al. In addition, the particle size of Al₂O₃ is highest for W_{Ti}^2 among others. These Al₂O₃ particles which act as dispersoids in the Al matrix, will influence the microstructure (grain structures) slightly differently. On annealing, the bigger Al₂O₃ dispersoids may impose smaller stabilizing effect on the low angle grain boundaries of Al [10]. The microstructural features which will be slightly different in the case of W_{Ti}^2 can affect the mechanism of the critical current flowing through the wire, and hence gets reflected on the I_c -B curve which has a slightly different slope than the other two wires. Fig. 9c compares the critical currents of the wires having the same characteristics of the (Al + Al₂O₃) sheath, but differing only by the barrier material (Ta or Ti) and slightly by the heat treatment temperature. As one can observe, both the wires sheathed by Al+1.5 vol % Al₂O₃ have nearly the same slope of $I_c(B)$ ($\frac{dI_c}{dB} = -0.3$).

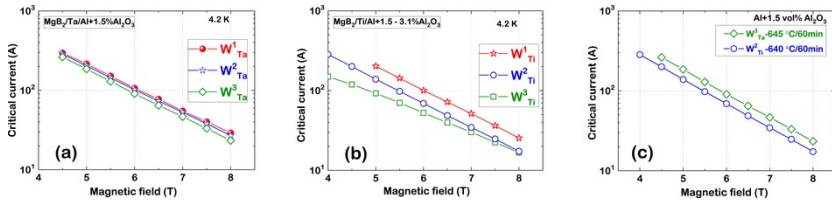


Fig. 9 Critical currents of (a) MgB₂-Ta-Al+1.5%Al₂O₃ wires and (b) MgB₂-Ti-Al+1.5-3.1%Al₂O₃. (c) Comparison of I_c for the W_{Ta}^3 and W_{Ti}^2 wires which have similar heat treatment conditions and with same Al purity and 1.5 vol% Al₂O₃.

alt-text: Fig. 9

The thermal stability of the wires with Ta and Ti barriers was evaluated by measuring the current-voltage, I - V , characteristic curves above the 1 μ V (criterion for critical current) as shown in Fig. 10a and b respectively. Apparent are the effects of applied heat treatments and the outer (Al + Al₂O₃) stabilizer sheaths on I - V curves, reflecting the transport current flow through the TaAl₃ or TiAl₃ phases and dominantly inside the outer (Al + Al₂O₃) sheaths. The voltage in the wires with Ta barrier increases more radically with current than for the ones with Ti barrier. Comparing Fig. 10a and b, we notice that the difference between the total excluding of transport current from MgB₂ (shown by an arrow up) and returning back (shown by an arrow down) is larger for the wires with Ta barrier. It also indicates different resistivity of the annealed sheaths. By comparison, the linear I - V characteristic of wires with the same sheath, W_{Ti}^2 wire with Ti barrier exhibits better thermal stability at 4.2 K and 7 T than W_{Ta}^3 , see Fig. 10c. It reflects the sheath resistance at 4.2 K (0.181 $\mu\Omega$ - W_{Ti}^2 and 0.321 $\mu\Omega$ - W_{Ta}^3), which also correlates well with the resistances shown in Fig. 8b.

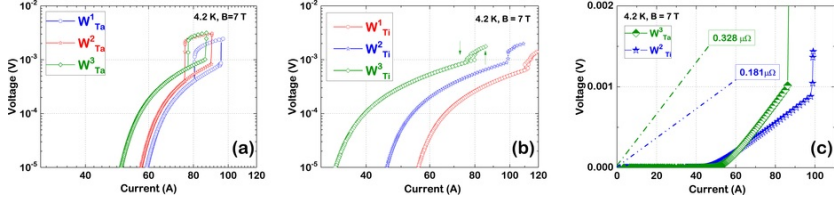


Fig. 10 I - V characteristic curves of (a) MgB₂-Ta-Al + Al₂O₃ wires and (b) MgB₂-Ti-Al + Al₂O₃ wire measured at the constant ramp rate of transport current 0.33 As⁻¹ in external field 7 T. (c) Comparison of I - V characteristics for W_{Ta}^3 and W_{Ti}^2 with the same sheath material using a linear plot.

alt-text: Fig. 10

Therefore, we conclude that the MgB₂ wires with Ti diffusion barrier will help achieving better thermal stability than those with Ta owing to lower resistance of the outer stabilizer (Al + Al₂O₃) sheath, which can be a reason of Ti gathering the impurities form (Al + Al₂O₃) in spite of exhibiting significantly higher interfacial reaction kinetics at Ti-(Al + Al₂O₃).

4 Conclusions

The interfacial reaction behaviour of the (Al + Al₂O₃) sheath with Ta or Ti diffusion barrier is studied as a function of heat treatment conditions, Al purity and variability of Al₂O₃ particles in the internal magnesium diffusion (IMD) processed MgB₂ wires. The following conclusions are made in this study:

- (i) The reaction of Ta and Ti with (Al + Al₂O₃) results in the interfacial reaction zone constituting oxygen-free TaAl₃ and TiAl₃ as the major phases along with a thin phase layer of oxygen containing TaAl and TiAl respectively. The wires with the Ta barrier produces considerably thinner yet non-uniform interfacial zones on reaction with the (Al + Al₂O₃) sheath than those with Ti. In contrast to the wires with Ta barrier which show no significant variation in the reaction kinetics at the barrier-sheath interface, those with Ti exhibit a significantly higher interfacial kinetics when react with the (Al + Al₂O₃) sheath with the maximum Al purity (~99.995%), followed by those with the lower Al purity and higher volume fraction of Al₂O₃ particles.
- (ii) Corroborating with the behaviour of reaction kinetics at the barrier-sheath interface, the critical currents do not vary much for the wires with Ta barrier in contrast to those of Ti. For the wires with Ti barrier, the highest critical current is offered by the one with the highest purity of Al and least for the one with highest volume fraction of Al₂O₃ particles. We suggest that the critical current of the MgB₂ composite wire is a function of the hardness of the (Al + Al₂O₃) sheath which in turn depends on the volume fraction and particle size of Al₂O₃.
- (iii) The thermal stability of the (Al + Al₂O₃) sheathed MgB₂ wire with Ti barrier is better than with Ta because of lower resistance at 4.2 K in spite of the slower interfacial reaction kinetics of Ta with (Al + Al₂O₃) sheath and absence of any detectible oxide phase inside the Ta barrier.

Acknowledgements

This work was supported by the research grants of the Slovak Scientific Agency project APVV-18-0271, and S. Santra would like to acknowledge Royal Society-SERB Newton fellowship for funding the research.

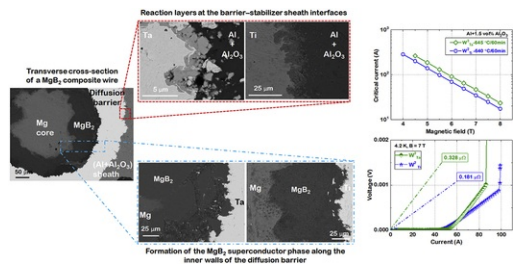
References

- [1] Y. Zenitani, J. Akimitsu, J. Nagamatsu, N. Nakagawa and T. Muranaka, Superconductivity at 39 K in magnesium diboride, *Nature* **410**, 2001, 63-64.
- [2] D.C. Larbalestier, L.D. Cooley, M.O. Rikel, A.A. Polyanskii, J. Jiang, S. Patnaik, X.Y. Cai, D.M. Feldmann, A. Gurevich, A.A. Squitieri, M.T. Naus, C.B. Eom, E.E. Hellstrom, R.J. Cava, K.A. Regan, N. Rogado, M.A. Hayward, T. He, J.S. Slusky, P. Khalifah, K. Inumaru and M. Haas, Strongly linked current flow in polycrystalline forms of the superconductor MgB₂, *Nature* **410**, 2001, 186-189.

- [3]** R. Flükiger, H.L. Suo, N. Musolino, C. Beneduce, P. Toulemonde and P. Lezza, Superconducting properties of MgB₂ tapes and wires, *Phys. C Supercond. its Appl.* **385**, 2003, 286–305.
- [4]** Y. Lvovsky, E.W. Stautner and T. Zhang, Novel technologies and configurations of superconducting magnets for MRI, *Supercond. Sci. Technol.* **26**, 2013, 093001.
- [5]** T.K. Hoang, L. Quéval, C. Berriaud and L. Vido, Design of a 20-MW fully superconducting wind turbine generator to minimize the levelized cost of energy, *IEEE Trans. Appl. Supercond.* **28**, 2018, 1–5.
- [6]** K. Togano, J.M. Hur, A. Matsumoto and H. Kumakura, Fabrication of seven-core multifilamentary MgB₂ wires with high critical current density by an internal Mg diffusion process, *Supercond. Sci. Technol.* **22**, 2009, 015003.
- [7]** I. Hušek, P. Kováč, T. Melišek and L. Kopera, Thermally stabilized MgB₂ composite wires with different barriers, *Cryogenics* **51**, 2011, 550–554.
- [8]** M. Parizh, Y. Lvovsky and M. Sumption, Conductors for commercial MRI magnets beyond NbTi: requirements and challenges, *Supercond. Sci. Technol.* **30**, 2016, 014007.
- [9]** B.A. Glowacki, M. Majoros, M. Vickers, M. Eisterer, S. Toenies, H.W. Weber, M. Fukutomi, K. Komori and K. Togano, Composite Cu/Fe/MgB₂ superconducting wires and MgB₂/YSZ/Hastelloy coated conductors for ac and dc applications, *Supercond. Sci. Technol.* **16**, 2003, 297–305.
- [10]** P. Kováč, I. Hušek, A. Rosová, M. Kulich, J. Kováč, T. Melišek, L. Kopera, M. Balog and P. Křížik, Ultra-lightweight superconducting wire based on Mg, B, Ti and Al, *Sci. Rep.* **8**, 2018, 2–8.
- [11]** P. Kováč, M. Balog, I. Hušek, L. Kopera, P. Křížik, A. Rosová, J. Kováč, M. Kulich and M. Čaplovičová, Properties of near- and sub-micrometre Al matrix composites strengthened with nano-scale in-situ Al₂O₃ aimed for low temperature applications, *Cryogenics* **87**, 2017, 58–65.
- [12]** W. Goldacker, S.I. Schlachter, S. Zimmer and H. Reiner, High transport currents in mechanically reinforced MgB₂ wires, *Supercond. Sci. Technol.* **14**, 2001, 787–793.
- [13]** C.R.M. Grovenor, L. Goodsir, C.J. Salter, P. Kováč and I. Hušek, Interfacial reactions and oxygen distribution in MgB₂ wires in Fe, stainless steel and Nb sheaths, *Supercond. Sci. Technol.* **17**, 2004, 479–484.
- [14]** P. Kováč, I. Hušek, T. Melišek, M. Kulich, A. Rosová, J. Kováč, L. Kopera, M. Balog, P. Křížik and L. Orovčík, Lightweight Al-stabilized MgB₂ conductor made by the IMD process, *Supercond. Sci. Technol.* **30**, 2017, 115001.
- [15]** <http://www.columbussuperconductors.com/>.
- [16]** <http://www.hypertechresearch.com/>.
- [17]** G. Z. Li, M. D. Sumption, M. A. Rindfleisch, C. J. Thong, M. J. Tomsic, and E. W. Collings, Enhanced higher temperature (20–30 K) transport properties and irreversibility field in nano-Dy₂O₃ doped advanced internal Mg infiltration processed MgB₂ composites, *Appl. Phys. Lett.* **105** (2014) 112603–1–4.
- [18]** D.L. Wang, Y.W. Ma, C. Yao, D. Xu, X. Zhang and S. Awaji, Transport properties of multifilament MgB₂ long wires and coils prepared by an internal Mg diffusion process, *Supercond. Sci. Technol.* **30**, 2017, 064003.
- [19]** P. Kováč, I. Hušek, E. Dobročka, T. Melišek, W. Haessler and M. Herrmann, MgB₂ tapes made of mechanically alloyed precursor powder in different metallic sheaths, *Supercond. Sci. Technol.* **21**, 2008, 015004.
- [20]** K. Das and S. Das, A review of the Ti–Al–Ta (titanium–aluminum–tantalum) system, *J. Phase Equilibria Diffusion* **26**, 2005, 322–329.
- [21]** N. Thiyaneshwaran, K. Sivaprasad and B. Ravisankar, Nucleation and growth of TiAl₃ intermetallic phase in diffusion bonded Ti/Al Metal Intermetallic Laminate, *Sci. Rep.* **8**, 2018, 16797.
- [22]** G.P. Kelkar and A.H. Karim, Phase equilibria in the Ti–Al–O system at 945 °C and analysis of Ti/Al₂O₃ reactions, *J. Am. Ceram. Soc.* **78**, 1995, 572–576.
- [23]** P. Kováč, I. Hušek, M. Kulich, J. Kováč, T. Melišek, L. Kopera, N. Perez, W. Haessler, M. Balog, P. Křížik and D. Berek, Lightweight MgB₂ wires with a high temperature aluminium sheath made of variable purity Al powder and Al₂O₃ content, *Supercond. Sci. Technol.* **31**, 2018, 085003.

Graphical abstract

Interfacial reaction at barrier-sheath and MgB₂ phase-formation, and current carrying capacities of Al + Al₂O₃ sheathed wire with Ta/Ti diffusion barriers.



alt-text: Image 1

Highlights

- Non-uniform, thinner interfacial layer for reaction of Al + Al₂O₃ with Ta than with Ti.
- Interfacial reaction at barrier-sheath do not govern critical current of MgB₂ wire.
- Critical current of Al + Al₂O₃ sheathed MgB₂ wire depends on Al purity, vol % of Al₂O₃.
- Thermal stability of MgB₂ wire with Ti barrier is better than the one with Ta.

Queries and Answers

Query: Please confirm that the provided email “sangeeta.santra@gmail.com” is the correct address for official communication, else provide an alternate e-mail address to replace the existing one, because private e-mail addresses should not be used in articles as the address for communication.

Answer: Yes, the email address is correct.

Query: Have we correctly interpreted the following funding source(s) and country names you cited in your article: SERB, India; Slovak Scientific Agency?

Answer: Yes

Query: Please confirm that given names and surnames have been identified correctly and are presented in the desired order and please carefully verify the spelling of all authors’ names.

Answer: Yes

Query: Your article is registered as a regular item and is being processed for inclusion in a regular issue of the journal. If this is NOT correct and your article belongs to a Special Issue/Collection please contact m.radhakrishnan@elsevier.com immediately prior to returning your corrections.

Answer: Yes